

ARTICLE OPEN



MECOM promotes leukemia progression and inhibits mast cell differentiation through functional competition with GATA2

Kohei Iida^{1,11}, Mayuko Nakanishi^{1,11}, Jakushin Nakahara¹, Shuhei Asada², Tomoya Isobe³, Tomohiro Yabushita⁴, Tsuyoshi Fukushima⁵, Yosuke Tanaka⁵, Manabu Ozawa^{6,7}, Yasuhiro Yamada⁸, Toshio Kitamura^{9,10}, Keita Yamamoto¹ and Susumu Goyama¹✉

© The Author(s) 2026

MECOM is a transcription factor critical for the maintenance of hematopoietic stem cells (HSCs) and the pathogenesis of myeloid leukemia. Germline mutations clustered in the C-terminal zinc finger domain (ZFD) of MECOM are known to cause MECOM-associated syndromes, involving bone marrow failure and skeletal anomalies. However, the molecular consequences of these mutations and the precise downstream mechanisms of MECOM remain elusive. Here, we demonstrate that the C-terminal ZFD serves as the dominant DNA-binding module of MECOM, and that disease-associated mutations abrogate its DNA-binding capacity. Mechanistically, we reveal that MECOM functionally antagonizes GATA2 via C-terminal ZFD-mediated DNA binding and recruitment of the corepressor CtBP. This repression promotes myeloid leukemogenesis while suppressing mast cell differentiation. Furthermore, we generated a knockin mouse model harboring a C-terminal ZFD mutation, which successfully recapitulated the clinical phenotypes of MECOM-associated syndromes, including reduction of HSCs and B cells. Collectively, our findings define C-terminal ZFD mutations as loss-of-function mutations with impaired DNA binding, uncover the MECOM-GATA2 axis as a key regulatory pathway, and provide a valuable mouse model for understanding MECOM-associated syndromes.

Leukemia; <https://doi.org/10.1038/s41375-026-02977-4>

INTRODUCTION

MECOM (MDS1 and EVI1 Complex Locus) is a PR domain family transcription factor essential for the maintenance of hematopoietic stem cells (HSCs) [1, 2]. While loss of MECOM impairs HSC generation and maintenance [3–5], its aberrant overexpression—driven by chromosomal translocations like *inv(3)(q21q26.2)*—triggers myelodysplastic syndrome (MDS) and acute myeloid leukemia (AML) [6]. High MECOM expression is also associated with therapeutic resistance and poor prognosis in AML [7, 8], underscoring its pivotal role in both normal and malignant hematopoiesis.

Structurally, MECOM contains N- and C-terminal zinc finger domains (ZFDs) with distinct DNA-binding specificities [9–11]. MECOM activates the transcription of several HSC-related genes, including GATA2, PBX1, and ERG [12–15]. It also functions as a transcriptional repressor for targets such as PTEN by recruiting transcriptional corepressors (C-terminal binding proteins: CtBPs) and epigenetic regulators (SUV39H1, G9a, and EZH2) [16–20]. In particular, CtBPs (CtBP1 and CtBP2) are implicated in MECOM-induced transcriptional repression and leukemogenesis. Despite these advances, the precise mechanisms of MECOM-mediated

transcription and transformation remain incompletely understood. For instance, it is unclear which ZFD is dominant for MECOM chromatin binding. Another unresolved issue is the complex relationship between MECOM and GATA2. GATA2 is a versatile transcription factor regulating multiple aspects of hematopoiesis, including HSC expansion and megakaryocyte/mast cell development [21–25]. While previous studies indicated that MECOM directly upregulates GATA2 to support HSC expansion during embryogenesis [5, 12], others have shown that 3q26.2 translocations reposition the GATA2 enhancer to the MECOM locus, causing MECOM overexpression with concurrent GATA2 downregulation [26, 27]. This clinical observation is supported by mouse models showing that *Gata2* haploinsufficiency accelerates MECOM-driven leukemogenesis [28, 29]. Thus, the role of GATA2 in MECOM-mediated hematopoiesis and leukemogenesis remains controversial and appears to be highly context-dependent.

Clinical relevance is further highlighted by the identification of germline *MECOM* mutations in “MECOM-associated syndromes,” which encompass Radial Ulnar Synostosis with Amegakaryocytic Thrombocytopenia (RUSAT) [30–35]. These pathogenic mutations are

¹Division of Molecular Oncology, Department of Computational Biology and Medical Sciences, Graduate School of Frontier Sciences, The University of Tokyo, Tokyo, Japan.

²Department of Radiation Oncology, Dana-Farber Cancer Institute, Harvard Medical School, Boston, MA, USA. ³Wellcome-MRC Cambridge Stem Cell Institute, Department of Hematology, University of Cambridge, England, UK. ⁴International Research Center for Medical Sciences, Kumamoto University, Kumamoto, Japan. ⁵Division of Cell Regulation, Center for Experimental Medicine and Systems Biology, The Institute of Medical Science, The University of Tokyo, Tokyo, Japan. ⁶Laboratory of Reproductive Systems Biology, Center for Experimental Medicine and Systems Biology, The Institute of Medical Science, The University of Tokyo, Tokyo, Japan. ⁷Core Laboratory for Developing Advanced Models, The Institute of Medical Science, The University of Tokyo, Tokyo, Japan. ⁸Department of Molecular Pathology, Graduate School of Medicine, The University of Tokyo, Tokyo, Japan. ⁹Institute of Biomedical Research Innovation, Foundation for Biomedical Research Innovation at Kobe, Kobe City, Japan. ¹⁰Molecular Pharmacology of malignant Diseases, Graduate School of Pharmaceutical Sciences, The University of Tokyo, Tokyo, Japan. ¹¹These authors contributed equally: Kohei Iida, Mayuko Nakanishi.

✉email: goyama@edu.k.u-tokyo.ac.jp

Received: 3 June 2024 Revised: 25 March 2026 Accepted: 20 April 2026

Published online: 05 May 2026

strikingly clustered in the C-terminal ZFD, suggesting this domain is fundamental to MECOM function. Although a recent mouse model harboring a C-terminal ZFD mutation recapitulated phenotypes like thrombocytopenia and HSC reduction [36], the specific molecular consequences of these mutations—particularly regarding DNA binding and target gene regulation—remain unknown.

Here, we dissected the molecular functions of the C-terminal ZFD and its interplay with CtBP. We demonstrate that the C-terminal ZFD is the dominant DNA-binding module of MECOM and that disease-associated mutations abolish this activity. We further reveal that MECOM functionally antagonizes GATA2 via C-terminal ZFD-mediated DNA binding and CtBP interaction. Finally, using a novel knock-in mouse model (R751W), we confirm that C-terminal ZFD mutations represent loss-of-function alleles that compromise HSC and B-cell development.

MATERIALS AND METHODS

Plasmids

Wild-type human MECOM (MECOM-WT) cDNA was obtained from DNA-FORM (Clone ID: 100067260, GenBank: BX647613.1) and cloned into pMYs-IRES-GFP (pMYs-IG) vector with a FLAG tag in the N-terminus between EcoRI and NotI sites. MECOM-DL/AS, MECOM-AS/AS, MECOM-R750W and MECOM-C766G mutants were produced by two-step PCR using the FLAG-MECOM-WT as a template. MECOM-WT with 3×HA tag was produced by PCR using the FLAG-MECOM-WT as a template. MECOM-WT and MECOM-R750W with AM tag were produced by PCR using FLAG-MECOM-WT and FLAG-MECOM-R750W as a template, respectively. Human CtBP1 cDNA was obtained from RIKEN BRC DNA Bank (Clone name: IRAL017H06, DDBJ: BC011655), and HA-tagged CtBP1 was cloned into pMYs-IRES-NGFR (pMYs-IN) vector between the EcoRI and NotI sites. FLAG-tagged human GATA2 was cloned into the pMYs-IN vector between the EcoRI and NotI sites. The pGL3-GATA-Luc containing 3× GATA promoter was obtained from Addgene (#85695). The pGL4-phCEBPA was provided by the RIKEN BRC through the National BioResource Project of the MEXT, Japan (cat. RDB07812). The +42 kb *CEBPA* enhancer region [37] was amplified by PCR from genomic DNA of MOLM13 cells. The PCR product was then cloned into pGL4-phCEBPA downstream of the luciferase gene at the MfeI and Sall sites using NEBuilder HiFi DNA Assembly Master Mix (New England Biolabs). Primers used are provided in Supplementary Table 1.

Mice

C57BL/6 (Ly5.2) mice (Japan SLC, Inc) were used for colony replating and bone marrow transplantation assays. Rosa26-LSL-Cas9 knock-in mice were purchased from Jackson Laboratory (#024857) [38]. To generate *Mecom*^{R751W/WT} knockin mice, Cas9 protein (IDT, Coralville, IA, USA), gRNA (5' ggggttccaagtgcctgtt 3', IDT) and single-stranded oligodeoxynucleotide (5' tgcgtggtggaacaacagctatgctgacttctctgtggtatattttcttcaaggctactgtggc aagatattccaaggctgctgcaATTaacaTggcacttgagaacccacagagagcaaccttca ggtagacagctgcttttcaaatctctcgataataactataatagcaatgctcattagctca 3', first two capital Ts or latter underlined single T represent silent mutations to delete PAM or R751W mutation in the KI allele, respectively, IDT) were electroporated into ES cells derived from B6-129F1 mice using Neon Electroporation System (Thermo Fisher, MI, USA). The completion of the desired KI was confirmed by genomic PCR followed by Sanger sequencing. Targeted ES cells were injected into blastocysts from ICR mice, and the injected blastocysts were transferred to the uterus of pseudopregnant ICR mothers to have chimeric offspring. The obtained chimeric mice were then crossed with C57BL/6 J mice, and offspring carrying the R751W allele were identified by genomic PCR followed by Sanger sequencing. Primers used for genomic PCR were as follows: *Mecom*_F: 5' acaaaattcaacaagatcgctaaagcagc 3', *Mecom*_R: 5' gaagaaaagacattctagttggaccctagcag 3'.

Cell culture

HEK293T and Plat-E cells were cultured in Dulbecco's Modified Eagle Medium (DMEM) (Fujifilm Wako Pure Chemical Co., Ltd., 044-29765), 10% fetal bovine serum (FBS) (Biosera), and 1% penicillin-streptomycin.

Western blotting and immunoprecipitation

HEK293T cells were transfected with the pMYs-IRES-GFP vector, Flag-tagged wild-type or mutant MECOM, and HA-tagged wild-type or mutant

CtBP1 using polyethylenimine (PEI). Cells were harvested 48 h after transfection and lysed in Cell Lysis Buffer (Cell Signaling Technology, Danvers, MA, USA; #9803). For immunoprecipitation, cell lysates were incubated with anti-FLAG antibody (SIGMA, F3165) for 30 min at 4 °C. Dynabeads-ProteinG (Invitrogen, USA; #10004D) was then added to the samples and incubated again for 30 min at 4 °C. After immunoprecipitation, samples were washed three times with Cell Lysis Buffer (Cell Signaling Technology, Danvers, MA, USA; #9803) containing 1 mM phenylmethanesulfonyl fluoride. Samples were then subjected to SDS-PAGE and transferred to a polyvinylidene fluoride membrane (Bio-Rad). The blot was incubated with anti-FLAG antibody (SIGMA, F3165) or anti-HA High-affinity antibody (Roche, 12CA5). Signals were detected with ECL Western Blotting Substrate (Promega, Madison, WI, USA) and visualized with Amersham Imager 600 (GE Healthcare) or LAS-4000 Luminescent Image Analyzer (FUJIFILM).

Immunostaining

293 T cells were transfected with the pMYs-IRES-GFP vector, FLAG-tagged wild-type or mutant MECOM. Forty-eight hours after transfection, the cells were fixed with 4% paraformaldehyde for 15 min at room temperature. The cells were then permeabilized with 0.2% Triton X-100 for 5 min and blocked with BSA for 1 h. Cells were fluorescently labeled with an anti-FLAG antibody (Sigma, F3165 or F7425) as the primary antibody and an anti-mouse antibody conjugated to Alexa Fluor 568 (Thermo Fisher, A11030) as the secondary antibody. Cell nuclei were stained with DAPI (BioLegend, catalog 422801). Fluorescence images were analyzed on an EVOS imaging system (Invitrogen).

Luciferase assay

293 T cells were seeded in 12-well culture plates at a density of 1×10^5 cells per well 18 h before transfection. For the luciferase assay with the CEBPA promoter/enhancer, the cells were transfected with pGL4-phCEBPA+42 kb enhancer together with pMYs-IG vector, pMYs-IG-MECOM-WT, pMYs-IG-MECOM-DL/AS, pMYs-IG-MECOM-R750W, or pMYs-IG-MECOM-C766G using polyethylenimine (PEI). For the luciferase assay with the GATA consensus sites, the cells were transfected with pGL3 containing three repeats of the GATA consensus site (Addgene #85695) and pGL4.74 vector together with pMYs-IN vector or pMYs-NGFR-GATA2 and pMYs-IG vector, pMYs-IG-MECOM-WT, pMYs-IG-MECOM-DL/AS, pMYs-IG-MECOM-R750W, or pMYs-IG-MECOM-C766G using PEI. Cells were harvested 48 h after transfection and were assayed for luciferase activity using the luciferase assay system (Promega) and a luminometer (BMG LABTECH, FLUOstar OPTIMA). Transfection efficiency was normalized using fluorometric quantitation of GFP.

Viral transduction

Retroviruses for mouse cells were generated by transfecting Plat-E packaging cells with the retroviral constructs using the calcium phosphate method [39]. Retroviruses for human cells were generated by transfecting HEK293T cells with RD114 (envelope) and M57 (gag-pol), along with the retrovirus constructs using the calcium phosphate method. Lentiviruses were generated by transfecting HEK293T cells with VSVG (envelope) (Addgene, #12259) and psPAX2 (gag-pol) (Addgene, #12260) along with the lentiviral constructs using the calcium phosphate method [40]. The medium was changed after 24 h, and the retroviral or lentiviral fluid was collected 48 h after transfection. The retroviruses were attached to a dish coated with RetroNectin (TaKaRa, #T100B) to infect the cells.

Flow cytometry

Cells were stained with fluorochrome-conjugated antibodies for 30 min at 4 °C, washed with PBS and resuspended in PBS containing 2% FBS. Cells were then analyzed by FACS Verse (BD Bioscience). The antibodies used are provided in Supplementary Table 2.

Colony replating, transplantation, and mast cell differentiation assays

Mouse bone marrow cells were collected from C57BL/6 (Ly5.2) female mice, 8 to 12 weeks old. Bone marrow progenitors (c-Kit⁺ cells) were selected using the CD117 MicroBead Kit (Miltenyi Biotec) and transduced with the pMYs-IRES-GFP vector, wild-type MECOM or MECOM mutants. For the colony replating assay, cells were grown in MethoCult™ M3234 (STEMCELL Technologies) with 10 ng/mL mouse stem cell factor (SCF) (R&D

Systems, 455-MC), 10 ng/mL mouse granulocyte macrophage colony-stimulating factor (R&D Systems, GM-CSF) (415-ML), 10 ng/mL mouse interleukin-3 (IL-3) (R&D Systems, 403-ML) and 10 ng/mL mouse interleukin-6 (IL-6) (R&D Systems, 406-ML). For each round of plating, 1×10^4 cells were plated. Colonies were counted and replated every 4 days. A colony was defined as a cluster of at least 50 cells.

For the transplantation assay, bone marrow c-Kit⁺ cells transduced with MECOM-WT, MECOM-DL/AS or MECOM-R750W were transplanted into sublethally (525 cGy) irradiated 12-week-old female C57BL/6 mice. Each mouse received 5×10^5 cells.

For the mast cell differentiation assay, bone marrow c-Kit⁺ cells were transduced with pMYS-IG vector, MECOM-WT, MECOM-DL/AS, MECOM-R750W and MECOM-C766G. After transduction, the cells were cultured in Iscove's Modified Dulbecco's Medium (IMDM) (Fujifilm Wako Pure Chemical Cooperation), 10% FBS (Biosera), 1% penicillin–streptomycin supplemented with murine 1 ng/ml IL-3, 10 ng/ml IL-6 and 100 ng/ml SCF (R&D Systems). The frequency of FcεR1a⁺c-Kit⁺ mast cells in the culture was evaluated by FACS every 3 days.

Morphological evaluation

1×10^4 cells were suspended in 100 μl PBS, and cell samples were prepared by cytopspin (650 rpm, 5 min). After centrifugation, adherent cells were dried on glass slides, fixed with methanol and stained with Maygimsa stain. Hemacolor[®] Rapid staining of blood smears (Millipore, #111956, #111957) was used for staining. Samples were observed using an Olympus BX51TF microscope.

Isolation and culture of human cord blood CD34⁺ cells

Mononuclear cells (MNCs) were isolated using Lymphoprep (Alera Technologies AS, Oslo, Norway). The CD34⁺ cell fraction was then isolated from the MNCs using the MidiMACS system (CD34+ Microbead Kit; Miltenyi Biotec; Bergisch Gladbach, Germany) according to the manufacturer's protocols. CB CD34⁺ cells were incubated in StemSpan[™] SFEMIL (STEMCELL Technologies) supplemented with 10 ng/ml mouse Flt-3, 10 ng/ml human thrombopoietin (TPO), 10 ng/ml human stem cell factor (SCF), 10 ng/ml human interleukin-3 (IL-3) and 10 ng/ml human interleukin-6 (IL-6) (R&D Systems).

Gata2 depletion using CRISPR/Cas9 in mouse bone marrow cells

To generate non-targeting (NT) or *Gata2*-targeting (sgGata2-A, B) short guide RNA (sgRNA) constructs, annealed oligos were inserted into the pLentiguide-puro vector, which was obtained from Addgene (#52963). Mouse bone marrow c-Kit⁺ cells from Rosa26-LSL-Cas9 knockin mice were transduced with the sgRNAs using the lentivirus and were selected for stable expression of the sgRNAs using puromycin (1 μg/ml) in MethoCult[™] M3234 (STEMCELL Technologies) supplemented with 10 ng/mL mouse SCF, 10 ng/mL mouse GM-CSF, 10 ng/mL mouse IL-3 and 10 ng/mL mouse IL-6 (R&D Systems). The efficiency of *Gata2* gene editing was assessed by the ICE CRISPR Analysis Tool (<https://ice.synthego.com/>). Sequences for the non-targeting (NT) control and sgRNAs targeting *Gata2* are provided as follows: NT: 5' cgcttccgcgcccgttcaa 3', sgGata2-A: 5' ggcgtccgcgcccgaagg 3', sgGata2-B: 5' caaccaccaccttatggcgc 3'.

RNA-Seq

For RNA-Seq with human CD34⁺ umbilical cord blood cells transduced with pMYS-IRE-GFP vector, wild-type MECOM, or mutant MECOM (MECOM-R750 or MECOM-DL/AS), GFP⁺ cells were sorted by FACS Aria III (BD Biosciences, San Jose, CA, USA) 48 h after transduction, and were cultured for 4 days as described above. Total RNA was then extracted and purified from the GFP⁺ cells using the FastGene[™] RNA Purification Kit (FastGene, FG-8005). Sequencing was then performed using Novaseq 6000. The fastq file was uploaded to Galaxy (<https://usegalaxy.org>) for analysis and mapped to the human genome (hg38) using HISAT2 [41]. Reads were then counted using Feature Count, and gene expression variations were analyzed using EdgeR [42]. The data generated by Feature Count were normalized by the TPM method, and then enrichment analysis (<https://maayanlab.cloud/Enrichr/>) was performed. The genes whose TPM value was less than 1 in all samples were removed as low-expression genes from the enrichment analysis and gene expression variation analysis.

For RNA-Seq with murine HSCs, bone marrow cells were collected from 8-week-old female littermate mice, and the SLAM-LSK (CD150⁺, CD48⁻, lineage⁻, Sca1⁺, cKit⁺) population was sorted directly into TRIZOL-LS using

FACS Aria III (BD Biosciences, San Jose, CA, USA). RNA extraction and RNA-seq were performed by Tsukuba i-Laboratory LLP using NextSeq500 (Illumina). The fastq file was imported into R (<https://www.r-project.org>) for analysis and mapped to the mouse reference genome (mm10). Reads were then counted using Feature Count, and the resulting data were normalized by the TPM method. Differentially expressed genes were identified using DESeq2 in R. Genes with an adjusted *p*-value < 0.05 were considered significantly differentially expressed.

Quantitative RT-PCR

Mouse bone marrow cells were transduced with pMYS-IG, MECOM-WT or MECOM-R750W. After transduction, the cells were cultured in MethoCult[™] M3234 (STEMCELL Technologies) with 10 ng/mL mouse SCF (455-MC), 10 ng/mL mouse GM-CSF (415-ML), 10 ng/mL mouse IL-3 (403-ML) and 10 ng/mL mouse IL-6 (406-ML) (R&D Systems). Total RNA was extracted using the RNeasy Mini kit (QIAGEN) 8 days after transduction and reverse transcribed using the High-Capacity cDNA Reverse Transcription Kit (Applied Biosystems). Complementary DNA (cDNA) was then subjected to quantitative RT-PCR using a SYBR Select Master Mix (Applied Biosystems). Sequences of the primers used are provided in Supplementary Table 1.

ChIP-Seq and ChIP-qPCR

293 T cells were transfected with pMYS-IG vector, MECOM-WT or MECOM-R750W with AM tag. Chromatin was then harvested, immunoprecipitated, and DNA purified using the SimpleChIP[®] Enzymatic Chromatin IP Kit (Magnetic Beads) (Cell Signaling, #9003). Anti-AM tag (active motif, catalog #91112) was used as the antibody for immunoprecipitation. Sequencing was performed on a next-generation sequencer from Chemical Dojin Co. The fastq file was uploaded to Galaxy (<https://usegalaxy.org>) for analysis and mapped to the human genome (hg38) using Bowtie2 (Galaxy Version 2.4.2+galaxy0) [43]. MACS2 (Galaxy Version 2.1.1.20160309.6) was used for peak calling [44]. ChIPseeker (Galaxy Version 1.18.0+galaxy1) was used for peak annotation [45]. BamCoverage (Galaxy Version 3.3.2.0.0), computeMatrix (Galaxy Version 3.5.1.0.0) and plotHeatmap (Galaxy Version 3.5.1.0.1) were used for sequence depth visualization [46]. The IGV tool (Version 2.8.12) was used to visualize sequence reads [47]. Homer (Version 4.10) was used to identify de novo motifs [48]. The size of the region used for motif discovery is 100 bp.

For ChIP-qPCR, purified DNA was subjected to quantitative RT-PCR after ChIP using a SYBR Select Master Mix (Applied Biosystems). The sequences of the primers used are provided in Supplemental Table 1.

Statistics

Statistical significance was determined by the indicated tests for independent variables using GraphPad Prism 9 (GraphPad Software Inc., La Jolla, CA). Statistical analyses to evaluate differences between two groups were performed using the unpaired *t*-test, One-way ANOVA with Dunnett's multiple comparisons test, Brown-Forsythe and Welch ANOVA with Dunnett's T3 multiple comparisons test, two-way ANOVA with Dunnett's multiple comparisons test, as described in the figure legends. The homogeneity of variance was confirmed among the groups analyzed by one-way and two-way ANOVA, followed by Dunnett's multiple comparisons test. Survival curves were compared using the log-rank test. For the *t*-test, the variance between the groups was assessed using the *F*-test. The sample size was determined based on prior experience and established practices in similar studies. For animal studies, the sample size was chosen to minimize the number of animals used while ensuring reproducibility of the findings. Samples or animals were excluded from the analysis only under specific conditions: (1) cell samples were excluded if contamination was detected during culture, and (2) animals were excluded if accidental death occurred due to unforeseen circumstances unrelated to the experimental procedures. No randomization and blinding were performed in this study due to the nature of the experimental design, which required direct observation and intervention by the investigator.

Ethics approval and consent to participate

All methods were performed in accordance with the relevant guidelines and regulations. Human umbilical cord blood (CB) was obtained from the Kanto-Koshinetsu Umbilical Cord Blood Bank of the Japanese Red Cross Society. Proper informed consent was obtained, and all experiments were performed according to an institutional review board-approved protocol (approval number: 27-34-1225, 2023-3-0508), in accordance with the

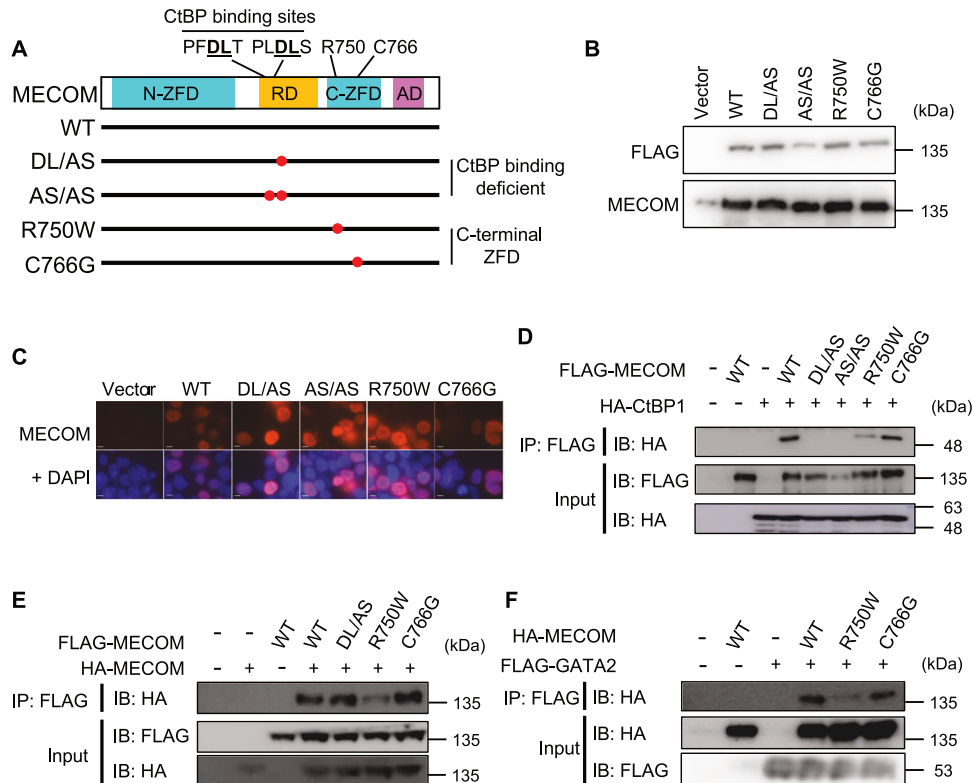


Fig. 1 Biochemical characterization of wild-type and mutant MECOM. Schematic of wild-type (WT) and mutant MECOM. DL/AS and AS/AS lose the interaction with CtBP by carrying 1 or 2 mutations in the CtBP binding sites. R750W and C766G have mutations in the C-terminal zinc finger domain (C-ZFD), which have been reported in MECOM-associated syndromes. N-ZFD: N-terminal ZFD, RD: Repression Domain, AD: Activation Domain (A). 293 T cells were transfected with vector or FLAG-tagged WT or mutant MECOM. MECOM levels were assessed by Western blotting with anti-FLAG or anti-MECOM antibodies (B). Cellular localization of WT or mutant MECOM was assessed by immunofluorescence with anti-FLAG antibody. Scale bars, 10 μ m; \times 1000 magnification (C). 293 T cells were transfected with FLAG-tagged WT or mutant MECOM together with HA-tagged CtBP1 (D) or HA-tagged MECOM (E). Cell lysates were immunoprecipitated with anti-FLAG antibody, followed by immunoblotting with anti-HA antibody. F 293 T cells were transfected with HA-tagged WT or mutant MECOM together with FLAG-tagged GATA2. Cell lysates were immunoprecipitated with anti-FLAG antibody, followed by immunoblotting with anti-HA antibody.

Declaration of Helsinki and The Belmont Report. All animal experiments were approved by the Animal Care Committee of the Institute of Medical Science at the University of Tokyo (PA21-67), and were conducted following the Regulation on Animal Experimentation at the University of Tokyo based on International Guiding Principles for Biomedical Research Involving Animals.

RESULTS

Biochemical characterization of MECOM mutants

We first generated a series of MECOM mutants to assess the impact of mutations in the C-terminal ZFD and CtBP-binding sites. These included the patient-derived C-terminal ZFD mutants R750W and C766G [30–35], as well as mutants disrupting one (DL/AS) or both (AS/AS) CtBP-binding motifs (Fig. 1A). All mutants showed comparable expression levels and nuclear localization to wild-type MECOM (Fig. 1B, C).

We next evaluated their protein-protein interaction properties. Consistent with prior studies [17, 20, 49], wild-type MECOM homodimerized and interacted with CtBP1. While CtBP-binding site mutants (DL/AS and AS/AS) lost CtBP1 binding as expected, the C-terminal ZFD mutant R750W—but not C766G—exhibited significantly reduced binding to both CtBP1 and wild-type MECOM (Fig. 1D, E). Additionally, we identified GATA2 as an interaction partner of MECOM, and this interaction was similarly impaired by the R750W mutation (Fig. 1F). These results indicate that among the C-terminal ZFD mutations tested, the R750W mutation uniquely impairs the protein-protein interaction capability of MECOM.

C-terminal ZFD and CtBP-binding site mutations abrogate MECOM oncogenic potential

We next assessed the biological consequences of these mutations using functional assays. In a serial colony replating assay using mouse c-Kit⁺ bone marrow progenitors, retroviral transduction of wild-type MECOM efficiently immortalized cells, sustaining colony formation through multiple rounds. In contrast, mutations in either the C-terminal ZFD or the CtBP-binding sites completely abrogated this replating capacity, despite comparable expression levels (Fig. 2A–C).

Consistent with the *in vitro* data, transplantation of mouse c-Kit⁺ bone marrow progenitor cells expressing wild-type MECOM into irradiated mice led to the expansion of GFP⁺ cells, significant thrombocytopenia (Fig. 2D), and lethal AML development within one year (Fig. 2E and Supplementary Fig. 1A–C). However, most mice receiving MECOM-R750W or MECOM-DL/AS transduced cells remained disease-free, confirming the loss of leukemogenic activity *in vivo* (Fig. 2E).

Finally, we examined the impact on the self-renewal capacity of human HSCs using cord blood (CB) CD34⁺ cells. While wild-type MECOM blocked myeloid differentiation and maintained a CD34⁺/CD14⁻ immature population, this differentiation block was abolished in cells expressing MECOM-DL/AS, MECOM-R750W, or MECOM-C766G (Fig. 2F, G and Supplementary Fig. 2A, B). Collectively, these findings establish that the integrity of both the C-terminal ZFD and CtBP recruitment is essential for MECOM-mediated HSC self-renewal and leukemogenesis.

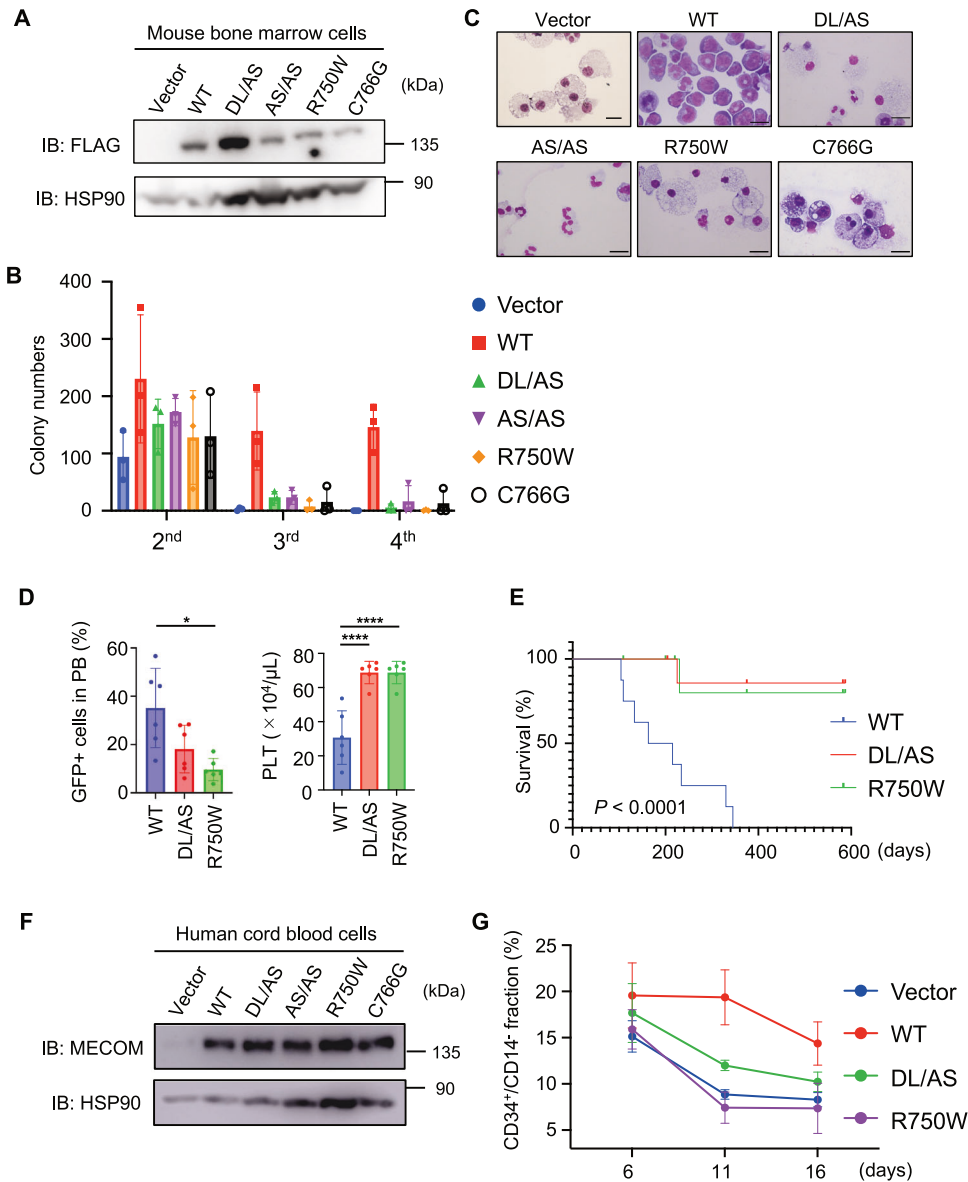


Fig. 2 Functional analysis of wild-type and mutant MECOM. Mouse bone marrow c-Kit⁺ cells were transduced with vector or FLAG-tagged wild-type (WT) or mutant (DL/AS, AS/AS, R750W, C766G) MECOM. Expression of each construct was confirmed by Western blotting with anti-FLAG and anti-HSP90 antibodies (A). Cells were serially replated every four days. Colonies were counted before replating (B, data are shown as mean with SD, $n = 3$). Representative images of each colony at the fourth round are also shown (C, Scale bars, 20 μ m; \times 1000 magnification). Mouse bone marrow c-Kit⁺ cells were transduced with WT or mutant (DL/AS or R750W) MECOM coexpressing GFP and transplanted into recipient mice. Peripheral blood data 1 month after transplantation (D, data are shown as mean with SD, * $P < 0.05$, **** $P < 0.0001$, Brown-Forsythe and Welch ANOVA with Dunnett's T3 multiple comparisons test for GFP, one-way ANOVA with Dunnett's multiple comparisons test for platelet counts, $n = 6$) and survival curves (E, $n = 8$ each, log-rank test) are shown. Human cord blood (CB) CD34⁺ cells were transduced with vector, WT, DL/AS, AS/AS, R750W and C766G (coexpressing GFP). Expression of each construct was confirmed by Western blotting with anti-MECOM and anti-HSP90 antibodies (F). Cells were cultured in myeloid skewing medium and analyzed by FACS to measure the frequency of CD34⁺/CD14⁻ cells (G, data are shown as mean with SD, $n = 3$).

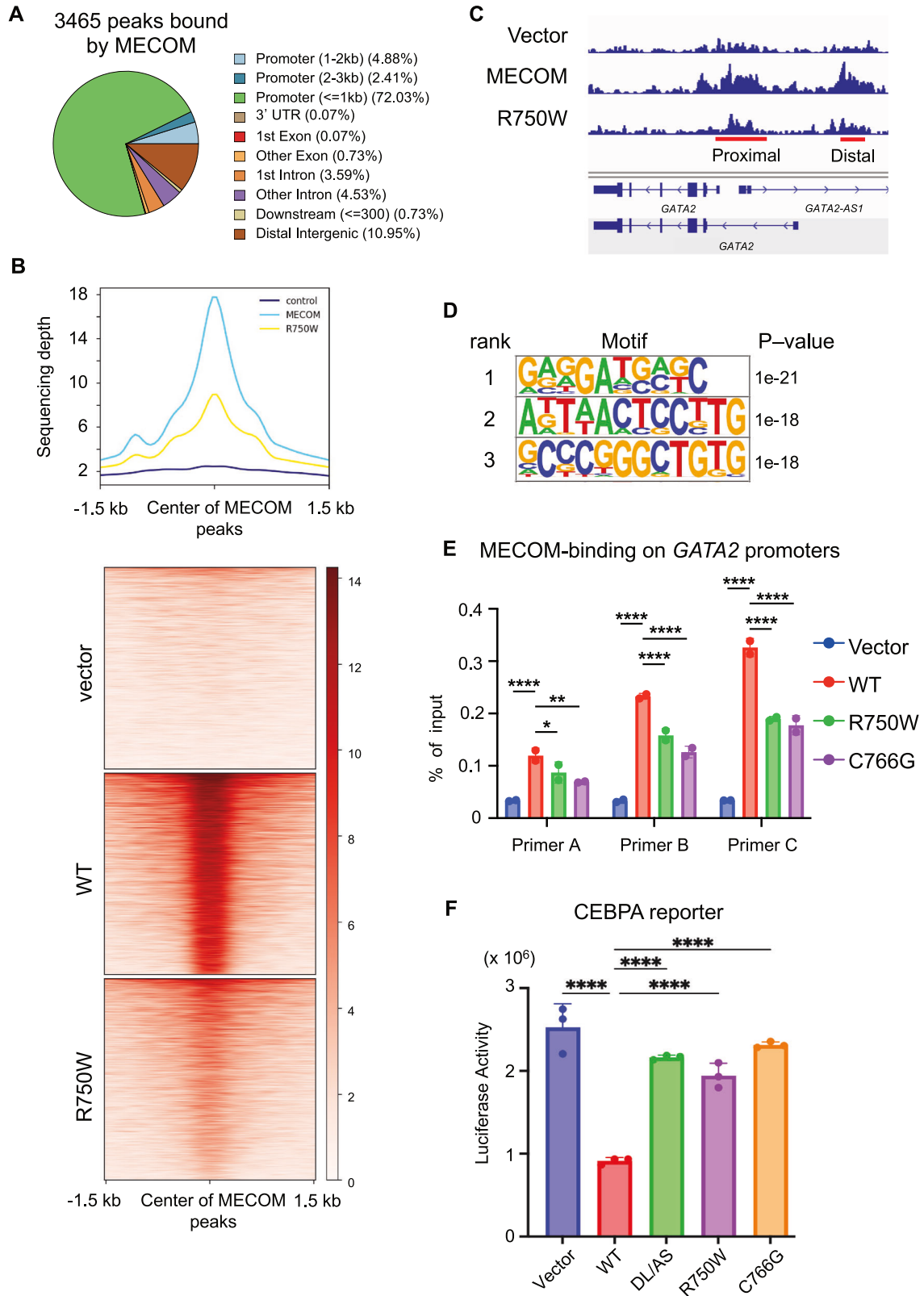
C-terminal ZFD mutations compromise DNA binding and transcriptional repression

Given that the R750W and C766G mutations are located within the C-terminal ZFD, a domain known for DNA binding, we hypothesized that these mutations impair MECOM's DNA-binding capability. To investigate this genome-wide, we performed ChIP-seq analysis using AM-tagged MECOM constructs in HEK293T cells (Supplementary Fig. 3A).

Wild-type MECOM showed robust binding to promoter regions of key target genes such as *GATA2* and *PBX1* (Fig. 3A–C and Supplementary Fig. 3B). Notably, the most significantly enriched motif closely resembled the known consensus sequence of the

C-terminal ZFD (5'-GAAGATGAG-3'), with no significant enrichment of the N-terminal ZFD motif (5'-GA(C/T)AAGA(T/C)AAGATAA-3') (Fig. 3D), indicating that the C-terminal ZFD is the dominant DNA-binding module. In contrast, MECOM-R750W exhibited significantly weaker binding to these targets despite occupying similar genomic loci (Fig. 3B, C and Supplementary Fig. 3B). ChIP-qPCR analysis further confirmed the reduced occupancy of both MECOM-R750W and MECOM-C766G at the *GATA2* promoter (Fig. 3E and Supplementary Fig. 3C).

Functionally, this loss of DNA binding translated to impaired transcriptional repression. In luciferase reporter assays using the *CEBPA* promoter, both MECOM-R750W and MECOM-C766G showed



significantly reduced repressive activity. Additionally, the MECOM-DL/AS mutant failed to repress transcription, confirming that CtBP recruitment is indispensable for this function (Fig. 3F). Collectively, these results demonstrate that disease-associated mutations abolish MECOM function by disrupting C-terminal ZFD-mediated DNA binding.

MECOM represses the mast cell transcriptional program via the C-terminal ZFD and CtBP recruitment

To elucidate the downstream pathways regulated by MECOM, we performed RNA-seq on human CB CD34⁺ cells expressing wild-type or mutant MECOM. Principal component analysis (PCA) and

Fig. 3 Reduced DNA binding ability of mutant MECOM with C-terminal ZFD mutations. 293 T cells were transfected with vector, AM-tagged wild-type (WT) MECOM or MECOM-R750W, immunoprecipitated with anti-AMtag antibody, followed by sequencing analysis. Genomic distribution of anti-AMtag ChIP-seq peaks (A), density maps of ChIP-seq peaks (B), and sequence reads at the proximal and distal GATA2 promoter (C) are shown. D De novo motif analysis of wild-type MECOM ChIP-seq peaks (a 70 bp DNA sequence extracted from each significant peak) using the Homer application (ver4.10). E Binding of MECOM-WT and MECOM-R750W to the proximal GATA2 promoter was assessed by ChIP-qPCR using three independent primers (see also Supplementary Fig. 3C). Data are shown as mean with SD, * $P < 0.05$, ** $P < 0.01$, **** $P < 0.0001$, two-way ANOVA with Dunnett's multiple comparisons test, $n = 2$). F 293 T cells were transfected with vector, FLAG-tagged wild-type (WT) or mutant (DL/AS, R750W, C766G) MECOM (co-expressing GFP) together with the CEBPA reporter. Transfection efficiency was normalized using fluorometric quantitation of GFP. Luciferase assays were performed in triplicate, and data are shown as mean with SD, **** $P < 0.0001$, one-way ANOVA with Dunnett's multiple comparisons test, $n = 3$.

hierarchical clustering revealed distinct transcriptomic landscapes for each construct (Fig. 4A and Supplementary Fig. 4A). By comparing the expression profiles, we defined sets of genes specifically repressed or activated by wild-type MECOM but not by the R750W or DL/AS mutants (Fig. 4B and Supplementary Fig. 4B, C; Supplementary Table 3). Notably, enrichment analysis highlighted a significant suppression of mast cell-associated genes in wild-type MECOM-expressing cells (Fig. 4C). This repression was confirmed by qPCR for key mast cell markers such as HDC, CPA3, TPSB2, and MITF, whose expression was restored in mutant MECOM-expressing cells (Fig. 4D).

Integration of ChIP-seq and RNA-seq data identified direct MECOM targets (Supplementary Fig. 5). Among these, we focused on MITF, a master regulator of mast cell development (Fig. 4D and Supplementary Fig. 5A). We demonstrated that wild-type MECOM binds directly to the MITF promoter, whereas binding was significantly reduced for the C-terminal ZFD (R750W, C766G) mutants (Fig. 4E, F and Supplementary Fig. 5B). These findings establish MITF as a direct repression target of MECOM. In summary, wild-type MECOM actively suppresses the mast cell lineage program, and this repressive function is abrogated by mutations in the C-terminal ZFD or CtBP-binding sites.

MECOM antagonizes GATA2 to suppress mast cell differentiation

To determine the impact of MECOM on mast cell lineage commitment, we transduced mouse bone marrow c-Kit⁺ cells with wild-type or mutant MECOM and induced mast cell differentiation in vitro. By day 12, vector-transduced cells efficiently differentiated into FcεR1α⁺c-Kit⁺ mast cells. In contrast, wild-type MECOM profoundly blocked this differentiation, reducing the mast cell population to less than 10%. This differentiation block was relieved by mutations in either the C-terminal ZFD (R750W, C766G) or the CtBP-binding sites (DL/AS) (Fig. 5A, B).

We next tested whether MECOM could counteract GATA2-driven mast cell maturation. Co-transduction of GATA2 with wild-type MECOM resulted in a significant suppression of GATA2-induced differentiation. However, this antagonistic effect was markedly attenuated in cells expressing the MECOM mutants (R750W, H766G, and DL/AS), further supporting their loss-of-function status (Fig. 5C, D).

Mechanistically, we explored whether MECOM directly represses GATA2 transcriptional activity. In luciferase reporter assays with a GATA-responsive element, wild-type MECOM potently inhibited GATA2-dependent activation. This repression was significantly compromised in all tested mutants (Fig. 5E). Collectively, these data demonstrate that MECOM functions as a physiological antagonist of GATA2, suppressing mast cell differentiation via a mechanism dependent on both DNA binding and CtBP-mediated repression.

Gata2 depletion partially restores the colony replating ability of mutant MECOM

To determine if the inability to repress GATA2 underlies the loss of leukemogenic potential in MECOM mutants, we performed a rescue experiment using CRISPR/Cas9-mediated *Gata2* depletion.

Mouse bone marrow c-Kit⁺ progenitors from Cas9 knock-in mice were transduced with wild-type or mutant MECOM alongside sgRNAs targeting the *Gata2* C-terminal zinc finger domain, where the mutations found in MonoMAC syndromes are concentrated [50]. These cells were serially replated in semisolid media (Fig. 6A). Control cells (vector) failed to sustain colony formation regardless of *Gata2* targeting, indicating that GATA2 loss alone does not confer self-renewal. Similarly, *Gata2* depletion provided no additional advantage to wild-type MECOM-transformed cells. In contrast, *Gata2* knockdown partially rescued the colony-forming capacity of cells expressing the transformation-defective mutants MECOM-R750W and MECOM-DL/AS (Fig. 6B). Morphologically, these *Gata2*-depleted, mutant MECOM-expressing colonies consisted of immature and granulocytic cells (Fig. 6C and Supplementary Fig. 6A). Flow cytometric analysis revealed an expansion of the c-Kit^{low}/CD11b⁻ population, which is enriched for leukemia stem cell activity, and a concurrent reduction in the c-Kit^{high} mast cell-like population in these colonies compared to *Gata2*-intact controls (Fig. 6D and Supplementary Fig. 6B).

Sequencing of the *Gata2* locus in the resulting colonies confirmed the presence of indels in MECOM-R750W cells. Interestingly, we observed a lack of edited alleles in wild-type MECOM colonies, suggesting that further suppression of GATA2 in the context of wild-type MECOM might be detrimental (Supplementary Fig. 7). Collectively, these data indicate that the colony replating ability of MECOM relies, at least in part, on its ability to functionally antagonize GATA2.

Hematopoietic dysregulation in *Mecom*^{WT/R751W} mice

To define the physiological consequences of the R750W mutation, we generated a knock-in mouse model carrying the equivalent *Mecom* R751W mutation. While homozygosity resulted in embryonic lethality by E14.5 (Fig. 7A), heterozygous *Mecom*^{WT/R751W} mice were viable and displayed normal peripheral blood counts over 1.5 years (Supplementary Fig. 8).

Detailed immunophenotyping revealed a significant reduction in the HSC pool. Specifically, the frequency of lineage⁻Sca-1⁺c-Kit⁺ (LSK) cells in E14.5 fetal liver (Fig. 7B) and SLAMF7 long-term (LT)-HSCs in adult bone marrow (Fig. 7C) were decreased in *Mecom*^{WT/R751W} mice compared to littermate controls. Additionally, we noted a modest reduction in bone marrow B220⁺ B cells, with no significant changes in myeloid or erythroid lineages (Fig. 7D).

Transcriptomic analysis of sorted HSCs provided mechanistic insight into these defects. *Mecom*^{WT/R751W} HSCs showed downregulation of self-renewal genes (*Cyp26b1*, *Chd7*) [51, 52] and upregulation of cell cycle/stress genes (*Socs2*, *Cxcr4*) [53, 54]. Furthermore, the gene signature indicated a lineage skewing characterized by premature lymphoid priming (*Flt3*, *Tespa1* upregulation) [55, 56] and loss of megakaryocytic/erythroid potential (*P2rx1*, *Sox6* downregulation) [57, 58] (Fig. 7E and Supplementary Table 4). Collectively, these findings indicate that the R751W mutation disrupts HSC quiescence and lineage fidelity.

Thus, *Mecom*^{WT/R751W} mice successfully recapitulate key features of MECOM-associated syndromes, including HSC depletion and B-cell deficiency. The mild nature of the phenotype, however,

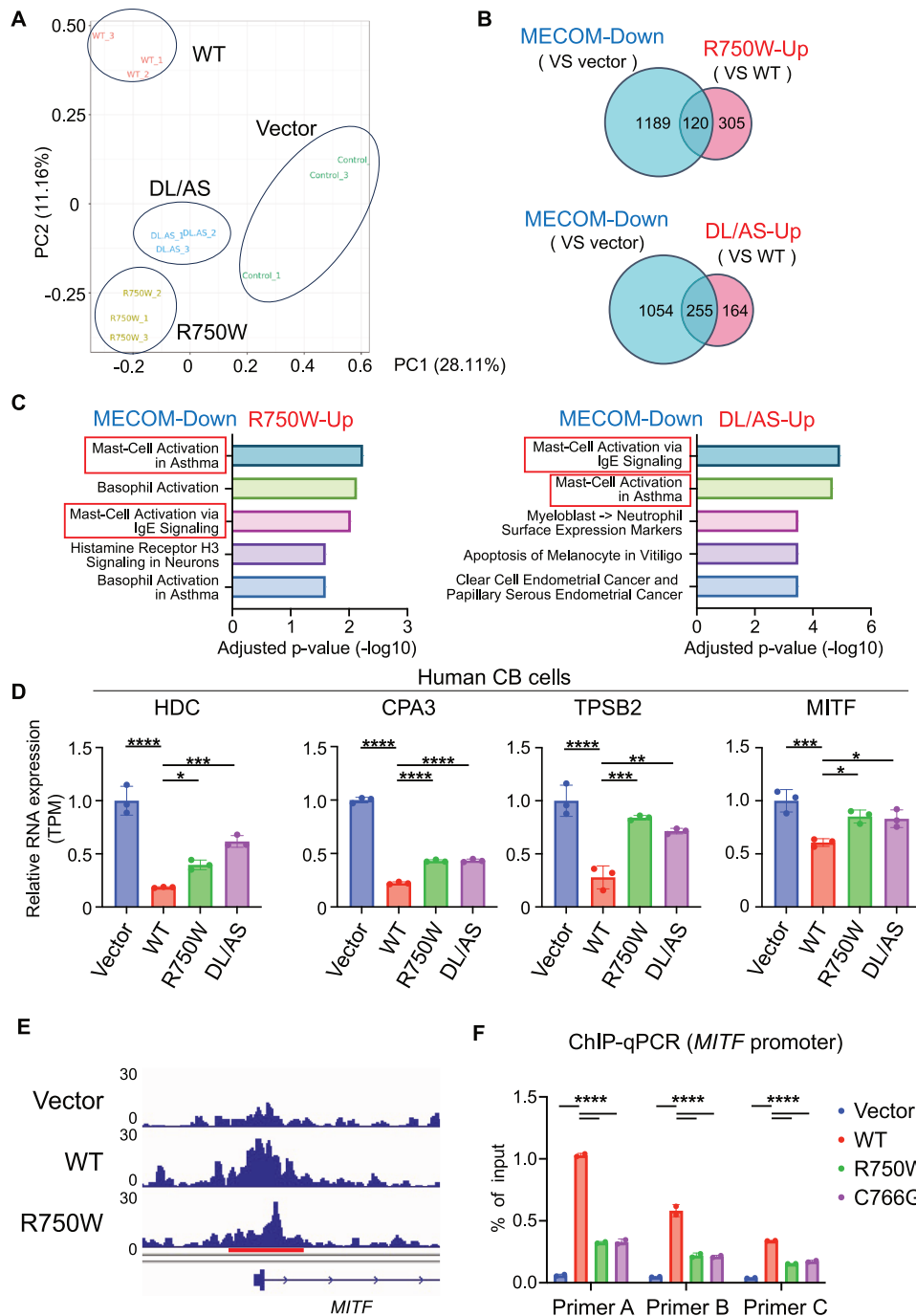


Fig. 4 Mast cell genes are repressed by wild-type, but not mutant, MECOM. Human cord blood (CB) CD34⁺ cells were transduced with vector, wild-type (WT) or mutant (DL/AS, R750W) MECOM coexpressing GFP. After 4 days of culture in stem cell medium, RNA was extracted from GFP⁺ cells and subjected to RNA-seq. **A** Principal Component Analysis (PCA) of RNA-seq data. **B** Venn diagram showing the genes downregulated in MECOM-WT-transduced CB cells compared to vector-transduced CB cells (blue circle) and genes upregulated in MECOM-R750W- (upper panel) or MECOM-DL/AS- (lower panel) transduced CB cells compared to MECOM-WT-transduced CB cells (red circle). Genes with FDR < 0.05 were considered as up- or down-regulated genes. **C** The 120 (for R750W) and 255 (for DL/AS) overlapping genes were used for enrichment analysis using Elsevier Pathway Collection. The mast cell-related gene sets are highlighted by the red boxes. **D** Transcripts Per Million (TPM) of mast cell-related genes (HDC, CPA3, TPSB2 and MITF) in vector, WT, or mutant MECOM-transduced CB cells. Data are shown as mean with SD, **P* < 0.05, ***P* < 0.01, ****P* < 0.001, *****P* < 0.0001, one-way ANOVA with Dunnett's multiple comparisons test. *n* = 3. **E** 293 T cells were transfected with vector, AM-tagged wild-type (WT) MECOM or MECOM-R750W, immunoprecipitated with anti-AM-tag antibody, followed by sequencing analysis. Sequence reads at the MITF promoter are shown. **F** 293 T cells were transfected with vector, AM-tagged MECOM-WT, R750W or C766G, immunoprecipitated with anti-AM-tag antibody, followed by qPCR using three primers designed for different regions in the MITF promoter (see also Supplementary Fig. 5B). Data are shown as mean with SD, *****P* < 0.0001, two-way ANOVA with Dunnett's multiple comparisons test, *n* = 2).

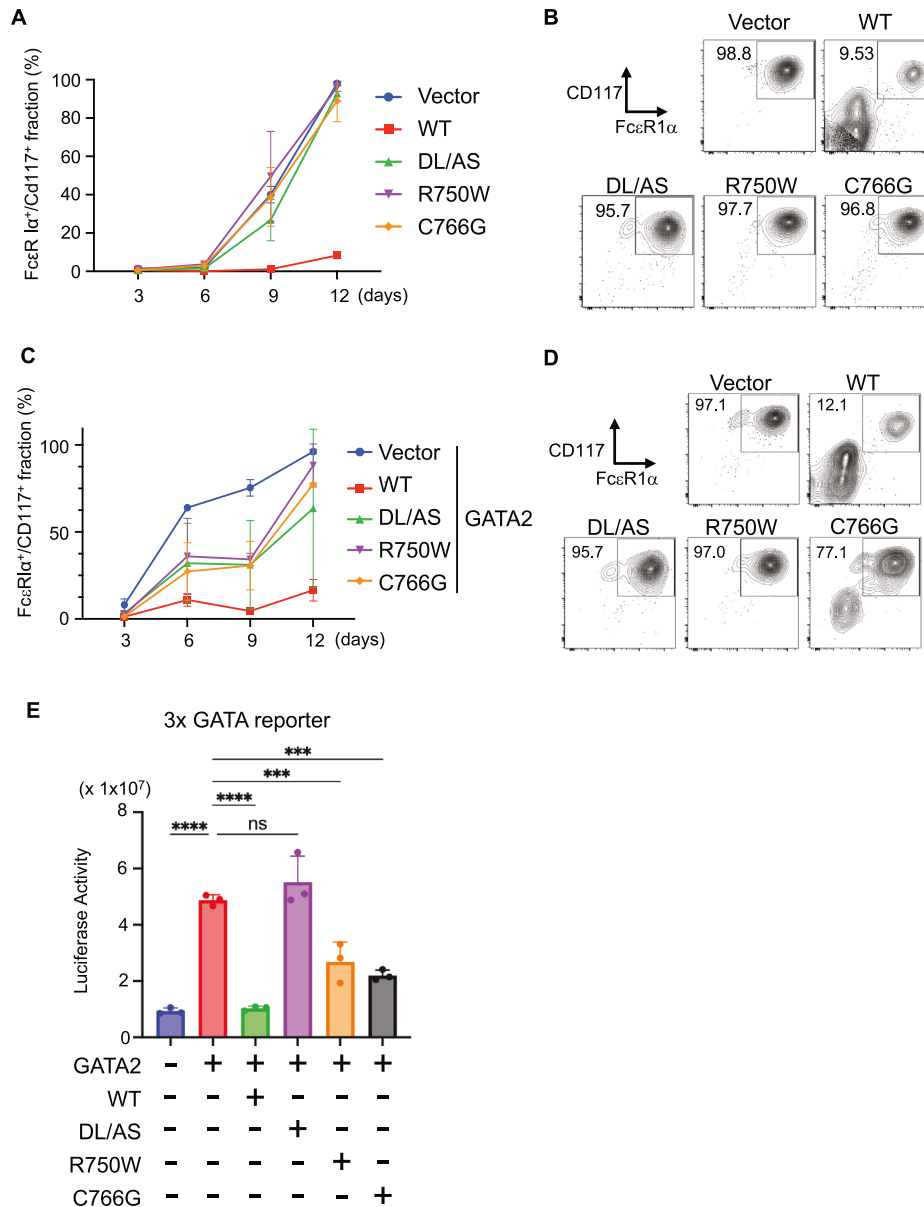


Fig. 5 MECOM inhibits GATA2 activity and mast cell differentiation. Mouse bone marrow $c\text{-Kit}^+$ cells were transduced with vector, wild-type (WT) or mutant (DL/AS, R750W, C766G) MECOM (coexpressing GFP) and cultured in the mast cell-inducing culture. The frequency of the mast cell fraction ($c\text{-Kit}^+/\text{Fc}\epsilon\text{R1}\alpha^+$) in GFP^+ cells was measured chronologically by FACS. Data are shown as mean with SD, $n = 2$ for each group (A). Representative FACS plots at day 12 are also shown. Numbers indicate the frequency (%) of $c\text{-Kit}^+/\text{Fc}\epsilon\text{R1}\alpha^+$ fraction in GFP^+ cells (B). Mouse bone marrow $c\text{-Kit}^+$ cells were transduced with vector, WT or mutant (DL/AS, R750W, C766G) MECOM (coexpressing GFP) together with vector or GATA2 (coexpressing NGFR) and cultured in the mast cell-inducing culture. The frequency of the mast cell fraction ($c\text{-Kit}^+/\text{Fc}\epsilon\text{R1}\alpha^+$) in $\text{GFP}^+/\text{NGFR}^+$ cells was measured chronologically by FACS. Data are shown as mean with SD, $n = 2$ for each group (C). Representative FACS plots at day 12 are also shown. Numbers indicate the frequency (%) of $c\text{-Kit}^+/\text{Fc}\epsilon\text{R1}\alpha^+$ fraction in $\text{GFP}^+/\text{NGFR}^+$ cells (D). E 293 T cells were transfected with vector, WT or mutant (DL/AS, R750W, C766G) MECOM (co-expressing GFP) together with GATA2 and the reporter plasmid containing 3x GATA sequences. Transfection efficiency was normalized using fluorometric quantitation of GFP. All luciferase assays were performed in triplicate, and data are shown as mean with **** $P < 0.0001$, *** $P < 0.001$, one-way ANOVA with Dunnett's multiple comparisons test, $n = 3$. ns: not significant.

implies that additional genetic or environmental modifiers may contribute to the full clinical spectrum of the disease.

DISCUSSION

MECOM is a critical transcription factor governing hematopoiesis, yet the functional impact of C-terminal ZFD mutations found in MECOM-associated syndromes [31–35] has remained elusive. Here, we demonstrate that mutations in this domain, exemplified by R750W and C766G, severely compromise DNA binding and

transcriptional activity. The global loss of genomic occupancy by MECOM-R750W identifies the C-terminal ZFD as the dominant DNA-binding module. Although the R750W mutation also affects protein-protein interactions, the fact that the C766G mutant retains these interactions but lacks transcriptional and transforming activities establishes DNA binding loss as the central driver of pathogenicity in these syndromes.

A key finding of our study is the antagonistic relationship between MECOM and GATA2. We show that MECOM represses GATA2-mediated transcription and blocks GATA2-driven mast cell

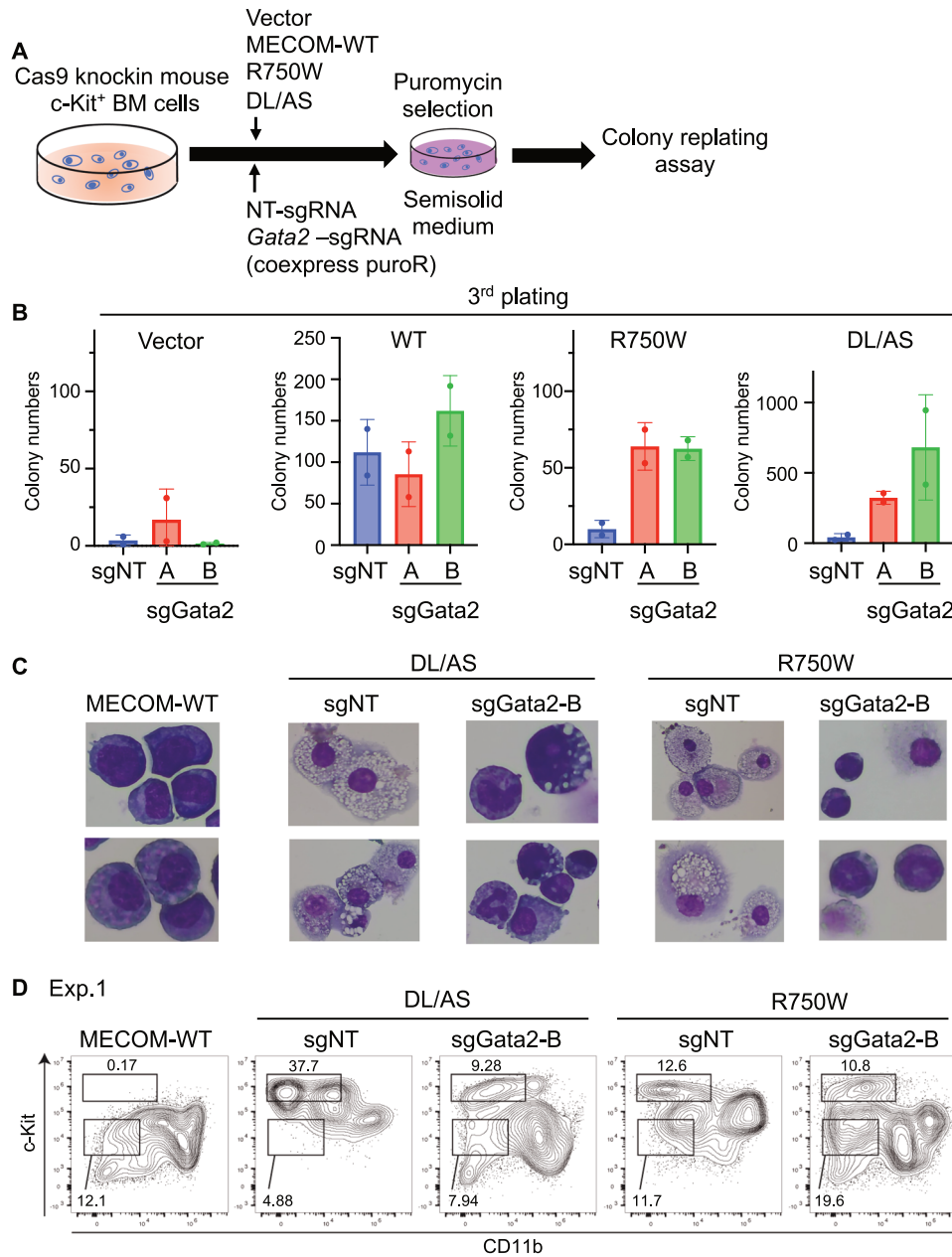


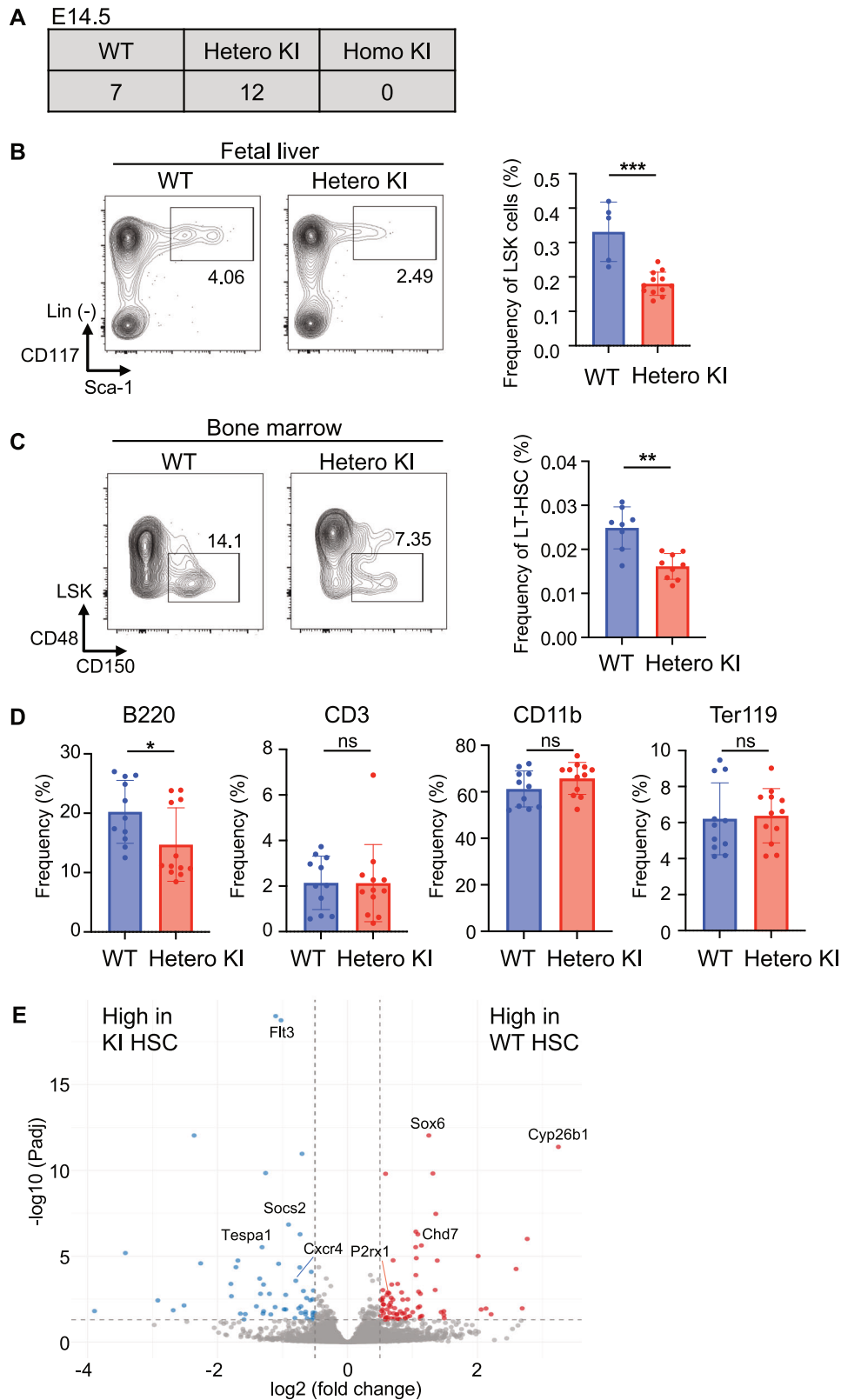
Fig. 6 **GATA2 depletion partially restores the colony replating ability of mutant MECOM.** **A** Experimental scheme used in **(B)**. Mouse bone marrow *c-Kit*⁺ cells derived from Cas9 knock-in mice were transduced with vector, wild-type (WT), R750W or DL/AS together with non-targeting (NT) or two independent *Gata2*-targeting sgRNAs [sgGata2-A and sgGata2-B coexpressing puromycin-resistant gene (PuroR)]. The sgRNA-transduced cells were selected with 1 mg/ml puromycin and were serially replated every four days. **B** Total colony numbers at the third plating. Data are shown as mean with SD, $n = 2$. Wright-Giemsa staining **(C)** and flow cytometric analysis **(D)** of colonies expressing MECOM mutants with/without *Gata2* depletion. The colonies expressing wild-type MECOM were also analyzed as controls. Numbers in **(D)** indicate the frequency of *c-Kit*^{high}*CD11b*⁻ and *c-Kit*^{low}*CD11b*⁺ populations in the colonies.

differentiation. Importantly, the leukemogenic defect of MECOM mutants could be partially rescued by *Gata2* depletion, reinforcing the concept that MECOM promotes leukemogenesis by restraining GATA2 function. This aligns with observations that *Gata2* haploinsufficiency accelerates MECOM-induced leukemia [28, 29]. While MECOM has been reported to upregulate *Gata2* in early hematopoiesis [5, 12], our data suggest a distinct, inhibitory mode of action in myeloid progenitors. This context-dependent duality of the MECOM-GATA2 axis represents a crucial area for future research.

Our *in vivo* analysis of *Mecom*^{WT/R751W} knock-in mice confirms that C-terminal ZFD mutations are loss-of-function alleles. Recapitulating features of *Mecom* null mice [3–5, 59],

homozygosity was lethal, while heterozygosity led to HSC and B-cell reduction, mirroring clinical observations. The phenotypic overlap with the recently described *Mecom*^{H752R} model [36] validates the pathogenicity of C-terminal ZFD mutations. However, subtle differences between models—such as the presence of thrombocytopenia in *Mecom*^{H752R} mice—suggest allele-specific effects that may underlie clinical heterogeneity. Furthermore, the mild nature of the murine phenotypes implies that additional genetic or environmental hits are likely necessary for the full manifestation of MECOM-associated syndromes.

In conclusion, we define C-terminal ZFD mutations as loss-of-function alleles defective in DNA binding. We propose a



mechanism whereby MECOM relies on this domain and CtBP recruitment to antagonize GATA2, thereby blocking differentiation and promoting leukemogenesis. Our findings and the newly

generated mouse model provide a solid foundation for understanding and targeting the molecular pathology of MECOM-associated disorders.

Fig. 7 Analysis of *Mecom*^{WT/R751W} knockin mice. **A** Genotypes of litters obtained by intercrossing *Mecom*^{WT/R751W} mice at embryonic (E) day 14. **B** Frequency of Lineage⁺Sca1⁺c-Kit⁺ (LSK) cells in fetal livers of wild-type (WT) and *Mecom*^{WT/R751W} mice at E14.5. Representative FACS plots (left, numbers indicate the frequency of LSK cells) and their quantification (right). Data are presented as mean with SD, ****P* < 0.001, unpaired and two-tailed Mann-Whitney test, WT mice: *n* = 5, *Mecom*^{WT/R751W} mice: *n* = 12). **C** Frequency of SLAM (CD150⁺CD48⁺) LSK cells in bone marrow of 2-month-old wild-type and *Mecom*^{WT/R751W} mice. Representative FACS plots (left, numbers indicate the frequency of SALM-LSK cells) and their quantification (right). Data are presented as mean with SD, ***P* < 0.01, unpaired and two-tailed Mann-Whitney test, WT: *n* = 8, *Mecom*^{WT/R751W} mice: *n* = 9). **D** Frequency of B220⁺, CD3⁺, CD11b⁺ and Ter119⁺ cells in bone marrow of mice analyzed in (C). Data are presented as mean with SD, **P* < 0.05, unpaired and two-tailed Mann-Whitney test, WT: *n* = 11, *Mecom*^{WT/R751W} mice: *n* = 12). **E** Volcano plot of RNA-seq data from sorted HSCs of wild-type (WT) and *Mecom*^{WT/R751W} mice. The x-axis indicates log₂ fold change (positive values indicate upregulation in wild-type), and the y-axis indicates statistical significance (−log₁₀ adjusted *P* value). Representative genes involved in HSC identity and lineage differentiation are labeled.

DATA AVAILABILITY

The RNA-seq and ChIP-seq data generated in this study have been deposited in the NCBI Gene Expression Omnibus (GEO) under accession numbers GSE324092, GSE322723, and GSE324091.

REFERENCES

- Goyama S, Kurokawa M. Pathogenetic significance of ecotropic viral integration site-1 in hematological malignancies. *Cancer Sci.* 2009;100:990–5.
- Goyama S, Kurokawa M. Evi-1 as a critical regulator of leukemic cells. *Int J Hematol.* 2010;91:753–7.
- Goyama S, Yamamoto G, Shimabe M, Sato T, Ichikawa M, Ogawa S, et al. Evi-1 is a critical regulator for hematopoietic stem cells and transformed leukemic cells. *Cell Stem Cell.* 2008;3:207–20.
- Kataoka K, Sato T, Yoshimi A, Goyama S, Tsuruta T, Kobayashi H, et al. Evi1 is essential for hematopoietic stem cell self-renewal, and its expression marks hematopoietic cells with long-term multilineage repopulating activity. *J Exp Med.* 2011;208:2402–15.
- Yuasa H, Oike Y, Iwama A, Nishikata I, Sugiyama D, Perkins A, et al. Oncogenic transcription factor Evi1 regulates hematopoietic stem cell proliferation through Gata-2 expression. *Embo J.* 2005;24:1976–87.
- Morishita K, Parganas E, Willman C, Whittaker M, Drabkin H, Oval J, et al. Activation of Evi1 gene-expression in human acute myelogenous leukemias by translocations spanning 300–400 kilobases on chromosome band-3q26. *Proc Natl Acad Sci USA.* 1992;89:3937–41.
- Van Doorn-Khosrovani S, Erpelinck C, Van Putten W, Valk P, De Luytgaarde S, Hack R, et al. High Evi1 expression predicts poor survival in acute myeloid leukemia: a study of 319 de novo AML patients. *Blood.* 2003;101:837–45.
- Lugthart S, Gröschel S, Beverloo H, Kayser S, Valk P, Van Zelderen-Bhola S, et al. Clinical, molecular, and prognostic significance of who type Inv(3)(Q21q26.2)/T(3;3)(Q21;Q26.2) and various other 3q abnormalities in acute myeloid leukemia. *J Clin Oncol.* 2010;28:3890–8.
- Perkins A, Fishel R, Jenkins N, Copeland N. Evi-1, A murine zinc finger proto-oncogene, encodes a sequence-specific DNA-binding protein. *Mol Cell Biol.* 1991;11:2665–74.
- Funabiki T, Kreider B, Ihle J. The carboxyl domain of zinc fingers of the Evi-1 myeloid transforming gene binds a consensus sequence of gaagatgag. *Oncogene.* 1994;9:1575–81.
- Delwel R, Funabiki T, Kreider B, Morishita K, Ihle J. 4 of the 7 zinc fingers of the Evi-1 myeloid-transforming gene are required for sequence-specific binding to Ga(C/T)Aaga(T/C)Aagataa. *Mol Cell Biol.* 1993;13:4291–300.
- Sato T, Goyama S, Nitta E, Takeshita M, Yoshimi M, Nakagawa M, et al. Evi-1 Promotes para-aortic splanchnopleural hematopoiesis through up-regulation of gata-2 and repression of Tgf-β signaling. *Cancer Sci.* 2008;99:1407–13.
- Shimabe M, Goyama S, Watanabe-Okochi N, Yoshimi A, Ichikawa M, Imai Y, et al. Pbx1 is a downstream target of Evi-1 in hematopoietic stem/progenitors and leukemic cells. *Oncogene.* 2009;28:4364–74.
- Masamoto Y, Chiba A, Mizuno H, Hino T, Hayashida H, Sato T, et al. Evi1 exerts distinct roles in Aml via Erg and cyclin D1 promoting a chemoresistant and immune-suppressive environment. *Blood Adv.* 2023;7:1577–93.
- Schmoeller J, Barbosa I, Minnich M, Andersch F, Smeenk L, Havermans M, et al. Evi1 drives leukemogenesis through aberrant ERG activation. *Blood.* 2023;141:453–66.
- Yoshimi A, Goyama S, Watanabe-Okochi N, Yoshiki Y, Nannya Y, Nitta E, et al. Evi1 represses pten expression and activates PI3k/Akt/Mtor via interactions with polycomb proteins. *Blood.* 2011;117:3617–28.
- Izutsu K, Kurokawa M, Imai Y, Maki K, Mitani K, Hirai H. The corepressor CtBP interacts with Evi-1 to repress transforming growth factor β signaling. *Blood.* 2001;97:2815–22.
- Pastoor D, Havermans M, Mulet-Lázaro R, Brian D, Noort W, Grasel J, et al. Oncogene Evi1 drives acute myeloid leukemia via a targetable interaction with Ctbp2. *Sci Adv.* 2024;10:eadk9076.
- Goyama S, Nitta E, Yoshino T, Kako S, Watanabe-Okochi N, Shimabe M, et al. Evi-1 interacts with histone methyltransferases Suv39h1 and G9a for transcriptional repression and bone marrow immortalization. *Leukemia.* 2010;24:81–8.
- Palmer S, Brouillet J, Kilbey A, Fulton R, Walker M, Crossley M, et al. Evi-1 trans-forming and repressor activities are mediated by CtBP co-repressor proteins. *J Biol Chem.* 2001;276:25834–40.
- Li Y, Gao J, Kamran M, Harmacek L, Danhorn T, Leach S, et al. Gata2 regulates mast cell identity and responsiveness to antigenic stimulation by promoting chromatin remodeling at super-enhancers. *Nat Commun.* 2021;12:494.
- Ohmori S, Moriguchi T, Noguchi Y, Ikeda M, Kobayashi K, Tomaru N, et al. Gata2 is critical for the maintenance of cellular identity in differentiated mast cells derived from mouse bone marrow. *Blood.* 2015;125:3306–15.
- De Pater E, Kaimakis P, Vink C, Yokomizo T, Yamada-Inagawa T, Van Der Linden R, et al. Gata2 is required for HSC generation and survival. *J Exp Med.* 2013;210:2843–50.
- Ling K, Ottersbach K, Van Hamburg J, Oziemlak A, Tsai F, Orkin S, et al. Gata-2 plays two functionally distinct roles during the ontogeny of hematopoietic stem cells. *J Exp Med.* 2004;200:871–82.
- Ikonomi P, Rivera C, Riordan M, Washington G, Schechter A, Noguchi C. Over-expression of Gata-2 inhibits erythroid and promotes megakaryocyte differentiation. *Exp Hematol.* 2000;28:1423–31.
- Yamazaki H, Suzuki M, Otsuki A, Shimizu R, Bresnick E, Engel J, et al. A remote Gata2 hematopoietic enhancer drives leukemogenesis in Inv(3)(Q21; Q26) by activating Evi1 expression. *Cancer Cell.* 2014;25:415–27.
- Gröschel S, Sanders M, Hoogenboezem R, De Wit E, Bouwman B, Erpelinck C, et al. A single oncogenic enhancer rearrangement causes concomitant Evi1 and Gata2 deregulation in leukemia. *Cell.* 2014;157:369–81.
- Yamaoka A, Suzuki M, Katayama S, Orihara D, Engel J, Yamamoto M. Evi1 and Gata2 misexpression induced by Inv(3)(Q21q26) contribute to megakaryocyte-lineage skewing and leukemogenesis. *Blood Adv.* 2020;4:1722–36.
- Katayama S, Suzuki M, Yamaoka A, Keleku-Lukwete N, Katsuoka F, Otsuki A, et al. Gata2 haploinsufficiency accelerates Evi1-driven leukemogenesis. *Blood.* 2017;130:908–19.
- Voit R, Sankaran V. Mecom deficiency: from bone marrow failure to impaired B-cell development. *J Clin Immunol.* 2023;43:1052–66.
- Germeshausen M, Ancliff P, Estrada J, Metzler M, Ponstingl E, Rüttschle H, et al. Mecom-associated syndrome: a heterogeneous inherited bone marrow failure syndrome with amegakaryocytic thrombocytopenia. *Blood Adv.* 2018;2:586–96.
- Osumi T, Tsujimoto S, Nakabayashi K, Taniguchi M, Shirai R, Yoshida M, et al. Somatic mecom mosaicism in a patient with congenital bone marrow failure without a radial abnormality. *Pediatr Blood Cancer.* 2018;65:e26959.
- Ripperger T, Hofmann W, Koch J, Shirnesan K, Haase D, Wulf G, et al. Mds1 and Evi1 complex locus (Mecom): a novel candidate gene for hereditary hematological malignancies. *Haematologica.* 2018;103:E55–8.
- Niihori T, Ouchi-Uchiyama M, Sasahara Y, Kaneko T, Hashii Y, Irie M, et al. Mutations in mecom, encoding oncoprotein Evi1, cause radioulnar synostosis with amegakaryocytic thrombocytopenia. *Am J Hum Genet.* 2015;97:848–54.
- Walne A, Tummala H, Ellison A, Cardoso S, Sidhu J, Sciuccati G, et al. Expanding the phenotypic and genetic spectrum of radioulnar synostosis-associated hematological disease. *Haematologica.* 2018;103:E284–7.
- Nagai K, Niihori T, Muto A, Hayashi Y, Abe T, Igarashi K, et al. Mecom mutation related to radioulnar synostosis with amegakaryocytic thrombocytopenia reduces Hspcs in mice. *Blood Adv.* 2023;7:5409–20.
- Avellino R, Havermans M, Erpelinck C, Sanders M, Hoogenboezem R, Van De Werken H, et al. An autonomous Cebpa enhancer specific for myeloid-lineage priming and neutrophilic differentiation. *Blood.* 2016;127:2991–3003.

38. Platt RJ, Chen SD, Zhou Y, Yim MJ, Swiech L, Kempton HR, et al. Crispr-Cas9 knock-in mice for genome editing and cancer modeling. *Cell*. 2014;159:440–55.
39. Kitamura T, Koshino Y, Shibata F, Oki T, Nakajima H, Nosaka T, et al. Retrovirus-mediated gene transfer and expression cloning: powerful tools in functional genomics. *Exp Hematol*. 2003;31:1007–14.
40. Goyama S, Schibler J, Gasilina A, Shrestha M, Lin S, Link KA, et al. Ubash3b/Sts-1-Cbl axis regulates myeloid proliferation in human preleukemia induced by Aml1-Eto. *Leukemia*. 2016;30:728–39.
41. Kim D, Landmead B, Salzberg SL. Hisat: a fast spliced aligner with low memory requirements. *Nat Methods*. 2015;12:357–U121.
42. Robinson MD, McCarthy DJ, Smyth GK. Edger: a bioconductor package for differential expression analysis of digital gene expression data. *Bioinformatics*. 2010;26:139–40.
43. Langmead B, Trapnell C, Pop M, Salzberg SL. Ultrafast and memory-efficient alignment of short DNA sequences to the human genome. *Genom Biol* 2009;10:R25.
44. Zhang Y, Liu T, Meyer CA, Eeckhoutte J, Johnson DS, Bernstein BE, et al. Model-based analysis of chip-seq (Macs). *Genom Biol*. 2008;9:R137.
45. Yu GC, Wang LG, He QY. Chipseeker: an R/bioconductor package for chip peak annotation, comparison and visualization. *Bioinformatics*. 2015;31:2382–3.
46. Ramírez F, Ryan DP, Grüning B, Bhardwaj V, Kilpert F, Richter AS, et al. Deeptools2: a next generation web server for deep-sequencing data analysis. *Nucleic Acids Res*. 2016;44:W160–5.
47. Robinson JT, Thorvaldsdóttir H, Winckler W, Guttman M, Lander ES, Getz G, et al. Integrative genomics viewer. *Nat Biotechnol*. 2011;29:24–6.
48. Heinz S, Benner C, Spann N, Bertolino E, Lin YC, Laslo P, et al. Simple combinations of lineage-determining transcription factors prime cis-regulatory elements required for macrophage and B cell identities. *Mol Cell*. 2010;38:576–89.
49. Nitta E, Izutsu K, Yamaguchi Y, Imai Y, Ogawa S, Chiba S, et al. Oligomerization of Evi-1, regulated by the pr domain, contributes to recruitment of corepressor Ctbp. *Oncogene*. 2005;24:6165–73.
50. Hsu A, Sampaio E, Khan J, Calvo K, Lemieux J, Patel S, et al. Mutations in Gata2 are associated with the autosomal dominant and sporadic monocytopenia and mycobacterial infection (Monomac) syndrome. *Blood*. 2011;118:2653–5.
51. Hsu J, Huang H, Lee C, Choudhuri A, Wilson N, Abraham B, et al. Chd7 and Runx1 interaction provides a braking mechanism for hematopoietic differentiation. *Proc Natl Acad Sci USA*. 2020;117:23626–35.
52. Schönberger K, Obier N, Romero-Mulero M, Cauchy P, Mess J, Pavlovich P, et al. Multilayer omics analysis reveals a non-classical retinoic acid signaling axis that regulates hematopoietic stem cell identity. *Cell Stem Cell*. 2022;29:131.
53. Vitali C, Bassani C, Chiodoni C, Fellini E, Guarnotta C, Miotti S, et al. Socs2 controls proliferation and stemness of hematopoietic cells under stress conditions, and its deregulation marks unfavorable acute leukemias. *Cancer Res*. 2015;75:2387–99.
54. Zhang Y, Dépond M, He L, Foudi A, Kwarteng E, Lauret E, et al. CXCR4/CXCL12 axis counteracts hematopoietic stem cell exhaustion through selective protection against oxidative stress. *Sci Rep*. 2016;6:37827.
55. Antar AI, Otrrock ZK, Jabbour E, Mohty M, Bazarbachi A. Flt3 inhibitors in acute myeloid leukemia: ten frequently asked questions. *Leukemia*. 2020;34:682–96.
56. Lu Y, Yang L, Shen M, Zhang Z, Wang S, Chen F, et al. Tespa1 facilitates hematopoietic and leukemic stem cell maintenance by restricting C-Myc degradation. *Leukemia*. 2023;37:1039–47.
57. Dumitriu B, Patrick M, Petschek J, Cherukuri S, Klingmuller U, Fox P, et al. Sox6 cell-autonomously stimulates erythroid cell survival, proliferation, and terminal maturation and is thereby an important enhancer of definitive erythropoiesis during mouse development. *Blood*. 2006;108:1198–207.
58. Ikeda M. Characterization of functional P2x1 receptors in mouse megakaryocytes. *Thromb Res*. 2007;119:343–53.
59. Hoyt P, Bartholomew C, Davis A, Yutzey K, Gamer L, Potter S, et al. The evil proto-oncogene is required at midgestation for neural, heart, and paraxial mesenchyme development. *Mech Dev*. 1997;65:55–70.

ACKNOWLEDGEMENTS

We thank Shiori Shikata and Akiho Tsuchiya for technical assistance. We also thank the Flow Cytometry Core and the Mouse Core at The Institute of Medical Science, The University of Tokyo.

AUTHOR CONTRIBUTIONS

KI designed and performed experiments, analyzed the data, and wrote the paper. MN designed and performed experiments and analyzed the data. JN, SA, TI and TY assisted in the experiments and analyzed the data. TF and YT assisted with the RNA-Seq with HSCs. MO and YY developed and provided chimera *Mecom*^{WT/R751W} mice. TK and KY conceived the project and analyzed the data. SG conceived the project, designed experiments, analyzed the data and wrote the paper.

FUNDING

This work was supported by Grant-in-Aid for Scientific Research (B) (23K24360, SG), Grant-in-Aid for Challenging Research (Exploratory) (24K22128, SG and KY), Fostering Joint International Research (B) (22KK0127, SG), AMED under Grant Number (22ck0106644s0202 and 23ama221514h0002, SG), the 36th Novartis Research Grant (SG), a research grant from the Daiichi Sankyo Foundation of Life Science (SG), research grants from The Japanese Society of Hematology (SG, TK), Grant-in-Aid for Scientific Research (A) (20H03537, TK), JSPS KAKENHI Grant Number JP24K19216 (KY), a research grant from The Mochida Memorial Foundation for Medical and Pharmaceutical Research (KY) and a research grant from The Uehara Memorial Foundation (KY), Grant-in-Aid for Japan Society for the Promotion of Science (JSPS) research fellow DC1 (24KJ0970, JN) and JST SPRING (JPMJSP2108, MN) from the Graduate School of Frontier Sciences, The University of Tokyo. Open Access funding provided by The University of Tokyo.

COMPETING INTERESTS

The authors declare no competing interests.

ADDITIONAL INFORMATION

Supplementary information The online version contains supplementary material available at <https://doi.org/10.1038/s41375-026-02977-4>.

Correspondence and requests for materials should be addressed to Susumu Goyama.

Reprints and permission information is available at <http://www.nature.com/reprints>

Publisher's note Springer Nature remains neutral with regard to jurisdictional claims in published maps and institutional affiliations.



Open Access This article is licensed under a Creative Commons Attribution-NonCommercial-NoDerivatives 4.0 International License, which permits any non-commercial use, sharing, distribution and reproduction in any medium or format, as long as you give appropriate credit to the original author(s) and the source, provide a link to the Creative Commons licence, and indicate if you modified the licensed material. You do not have permission under this licence to share adapted material derived from this article or parts of it. The images or other third party material in this article are included in the article's Creative Commons licence, unless indicated otherwise in a credit line to the material. If material is not included in the article's Creative Commons licence and your intended use is not permitted by statutory regulation or exceeds the permitted use, you will need to obtain permission directly from the copyright holder. To view a copy of this licence, visit <http://creativecommons.org/licenses/by-nc-nd/4.0/>.

© The Author(s) 2026